Energy Materials and Devices

Open Access
Research Article

Graphical Abstract

Supramolecular ligands enable efficient ion transport in solid-state lithium batteries

Qian-Nan Zhu†, Kang-Rui Ren†, Jun-Yao You, Zhen-Han Xie, Hai Su ✉, and Yan-Bing He ✉

Shenzhen Geim Graphene Center, Tsinghua Shenzhen International Graduate School, Tsinghua University, Shenzhen 518055, China

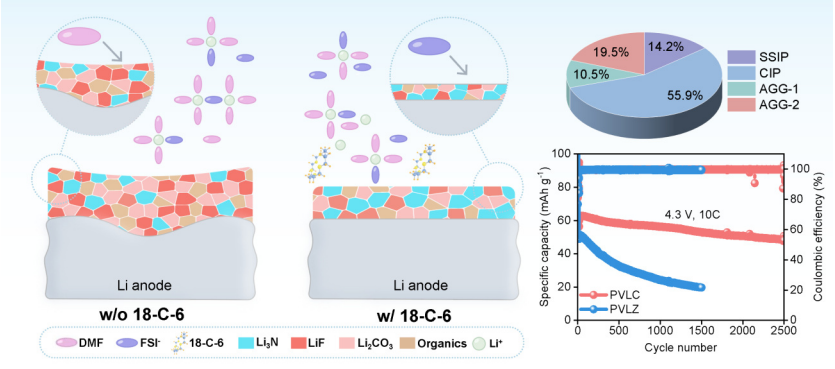

This study proposes a supramolecular ligand intervention strategy using 18-crown-6 as an additive. Coordination between large-pore crown ethers and Li^+ promotes LiFSI dissociation and increases the free Li^+ concentration, thereby enhancing ion transport with high ionic conductivity and an improved Li^+ transference number. Consequently, the modified poly(vinylidene fluoride)–lithium lanthanum zirconium oxide–crown ether (PVLC) electrolyte significantly enhanced the cycling stability of Li||Li cells up to 800 h with a reduced overpotential. The Li||NCM811 cells delivered 84.2% capacity retention over 2500 cycles at 10C. Even under a high cut-off voltage of 4.5 V at 5C, the cells retained 72.5% capacity after 780 cycles.

✉Address correspondence to
Hai Su, haisu@tju.edu.cn;
Yan-Bing He,
he.yanbing@sz.tsinghua.edu.cn

Received: April 7, 2026
Revised: May 2, 2026
Accepted: May 7, 2026

Read Online

Citation: Zhu Q., Ren K., You J., et al. Supramolecular ligands enable efficient ion transport in solid-state lithium batteries. *Energy Mater. Devices*, 2026, 4(2), 9370096. https://doi.org/10.26599/EMD.2026.9370096

Energy Materials and Devices
https://doi.org/10.26599/EMD.2026.9370096
Open Access
Research Article

Supramolecular ligands enable efficient ion transport in solid-state lithium batteries

Qian-Nan Zhu†, Kang-Rui Ren†, Jun-Yao You, Zhen-Han Xie, Hai Su ✉, and Yan-Bing He ✉

Shenzhen Geim Graphene Center, Tsinghua Shenzhen International Graduate School, Tsinghua University, Shenzhen 518055, China
† *Qian-Nan Zhu and Kang-Rui Ren contributed equally to this work.*

Cite this article: *Energy Mater. Devices* 2026, **4**(2): 9370096. https://doi.org/10.26599/EMD.2026.9370096

ABSTRACT

The development of poly(vinylidene fluoride)-based composite solid-state electrolytes is severely hindered by slow Li^+ transport and unstable solid-state electrolyte interphases. This study addresses these challenges by proposing a supramolecular ligand intervention strategy using 18-crown-6 as an additive. Coordination between the large-pore crown ethers and Li^+ promotes lithium bis(fluorosulfonyl)imide dissociation and increases the free Li^+ concentration, thereby enhancing ion transport with a high ionic conductivity and an improved Li^+ transference number. Moreover, this coordination homogenizes the Li^+ flux, suppressing side reactions and dendrite formation. Consequently, the modified electrolyte significantly enhances the cycling stability of Li||Li cells up to 800 h with a reduced overpotential. Additionally, the Li||NCM811 cells delivered 84.2% capacity retention after 2500 cycles at 10C, and retained 72.5% capacity after 780 cycles even at a high cut-off voltage of 4.5 V at 5C. Structural and interfacial characterizations confirmed the formation of a dense LiF/Li_3N-rich SEI layer, which enhances mechanical strength and ionic transport. This study provides a robust modification approach using supramolecular ligands to achieve high-performance solid-state lithium-metal batteries.

KEYWORDS

PVDF composite solid electrolyte, Li-salt dissociation, crown ether, Li^+ transport, solid-state lithium battery

1 Introduction

Lithium-metal batteries (LMBs), which integrate lithium-metal anodes—characterized by an extremely high theoretical capacity and the lowest redox potential[1, 2]—with high-voltage cathodes, such as $LiNi_{0.8}Co_{0.1}Mn_{0.1}O_2$ (NCM811), have attracted significant attention for their potential to achieve high energy density[3–5]. However, conventional liquid electrolytes present challenges, including uneven solid electrolyte interphase (SEI) formation, lithium dendrite growth, and inherent safety issues, when paired with lithium-metal anodes, severely limiting their practical applications[6–9]. Therefore, replacing flammable liquid electrolytes with inherently safer composite solid-state electrolytes (CSEs) has emerged as a viable strategy for overcoming these limitations[10, 11].

Poly(vinylidene fluoride) (PVDF)-based CSEs offer remarkable advantages, including excellent mechanical properties, superior thermal stability, and high ionic conductivity. They contain a small amount of *N*,*N*-dimethylformamide (DMF) that forms highly conductive $[Li(DMF)_x]^+$ coordination structures[12,13]. Nevertheless, electron transfer between DMF and the lithium-metal anode generates radicals, which continuously degrade interfacial stability[14]. Consequently, despite their acceptable ionic conductivity at room temperature, Li^+ diffusion within PVDF-based CSEs cannot sufficiently keep pace with Li plating. This kinetic mismatch facilitates uneven Li deposition at the interface and accelerated dendrite growth, ultimately compromising cycle stability[15,16]. Therefore, simultaneously enhancing the Li^+-transport capability and interface stability of these CSEs is critical to achieve high-performance LMBs. Numerous strategies have been explored, including Li-salt modification[17,18], polymer-matrix engineering[19,20], plasticizer and inorganic-filler incorporation[21], and artificial-SEI construction[22]. Specifically, the additive engineering of the electrolyte to form stable, compact interphase layers has attracted significant attention because such layers improve cell performance by effectively regulating Li-metal nucleation and growth while mitigating parasitic side reactions[23]. Nevertheless, the rational design of additives for PVDF-based CSEs still lacks adequate guidance, as interfacial behavior is simultaneously governed by the degree of Li-salt dissociation, the Li^+ coordination environment, and the chemical stability of the ligand molecules[24].

In this study, a large supramolecular ligand, 18-crown-6 (18-C-6), was proposed to modify PVDF/Ta-doped garnet-type lithium lanthanum zirconium oxide ($Li_{6.4}La_3Zr_{1.4}Ta_{0.6}O_{12}$, LLZTO) CSEs. The unique cyclic

Received: April 7, 2026 / **Revised:** May 2, 2026 / **Accepted:** May 7, 2026

✉**Address correspondence to** Hai Su, haisu@tju.edu.cn; Yan-Bing He, he.yanbing@sz.tsinghua.edu.cn

cavity of 18-C-6, along with the highly electronegative region created by internal oxygen atoms, effectively regulates the Li^+ coordination structure (Fig. 1)[25]. The larger cavity diameter of 18-C-6 relative to the ionic size of Li^+ (0.76 Å) provides a moderate coordination strength that effectively facilitates lithium bis(fluorosulfonyl)imide (LiFSI) dissociation and DMF substitution from the Li^+ solvation shell while preserving facile Li^+ decoordination and transport. Furthermore, the Li^+/18-C-6 cluster structures homogenize the Li^+ concentration at the anode interface, inducing the formation of a dense, uniform SEI layer, which effectively suppresses Li dendrite growth. Consequently, the modified PVDF-based CSE (PVDF–LLZTO–crown ether, PVLC) imparts the symmetrical lithium-metal cell (Li||Li) with stable cycling over 800 h with a small overpotential. To further evaluate its performance in high-energy-density systems, the PVLC electrolyte is integrated into the Li||NCM811 cell, significantly improving its cycling stability by delivering 570, 1200, and 2500 cycles at 2C, 5C, and 10C, respectively, and maintaining stability for nearly 800 cycles, even at a high cut-off voltage of 4.5 V.

2 Materials and methods

A self-supporting CSE was fabricated via a solution casting method. PVDF (400 mg), LiFSI (267 mg), and LLZTO (60 mg) were weighed and dispersed in DMF. Thereafter, the mixture was magnetically stirred to form a homogeneous solution, which was poured into a glass dish and transferred to a forced-air oven for hot-air drying to obtain the PVDF–LiFSI–LLZTO (PVLZ) electrolyte. In this study, PVLZ served as the control group. For the crown ether–containing electrolyte, PVDF (400 mg), LiFSI (267 mg), 18-C-6 (50 mg), and LLZTO (60 mg) were dissolved in DMF (15 mL) under identical conditions. After drying, the resulting electrolyte was labeled PVLC, representing the experimental group. The experimental procedures are detailed in the Electronic Supplementary Material (ESM).

3 Results and discussion

The morphology of solid-state electrolytes prepared via solution casting was characterized via scanning electron microscopy (SEM). The PVDF-based CSE exhibited characteristic large spherulites interspersed by abundant micron-scale voids, which significantly compromise electrolyte resistance to dendrite penetration (Fig. 2a). The incorporation of inorganic LLZTO fillers into the PVDF matrix (PVLZ electrolyte) effectively filled these interspherulitic voids, thereby decreasing the size of the polymer spherulites (Fig. 2b). Furthermore, 18-C-6 incorporation promoted the densification of the electrolyte film (Fig. 2c). Additionally, the cross-sectional SEM images of the PVLC CSE membrane revealed that the material exhibited a homogeneous thickness of approximately 90 μm, with the uniform dispersion of the inorganic fillers and no noticeable sedimentation (Fig. 2d).

Fourier transform infrared (FTIR) spectroscopy revealed that the characteristic β-phase (1070 and 1104 cm^{-1}) and γ-phase (833 cm^{-1}) peaks of PVDF in

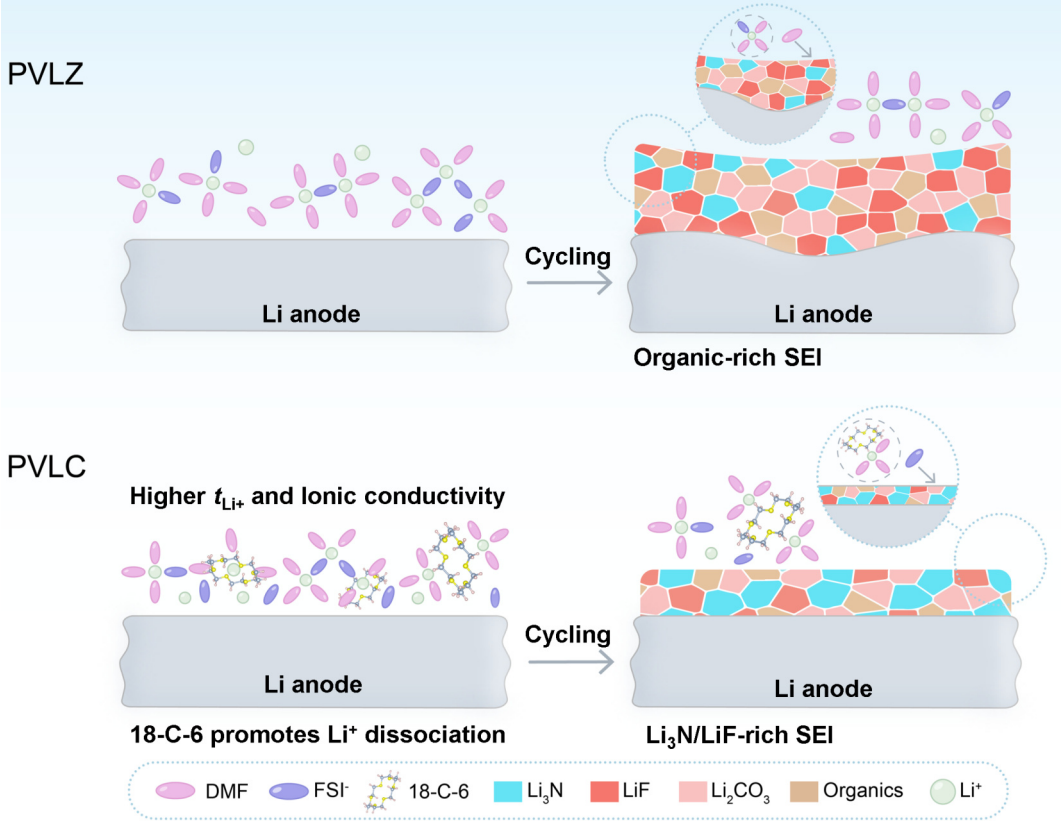

Figure 1 Schematic of the supramolecular ligands for enabling rapid Li^+ transport and stable solid electrolyte interphase (SEI).

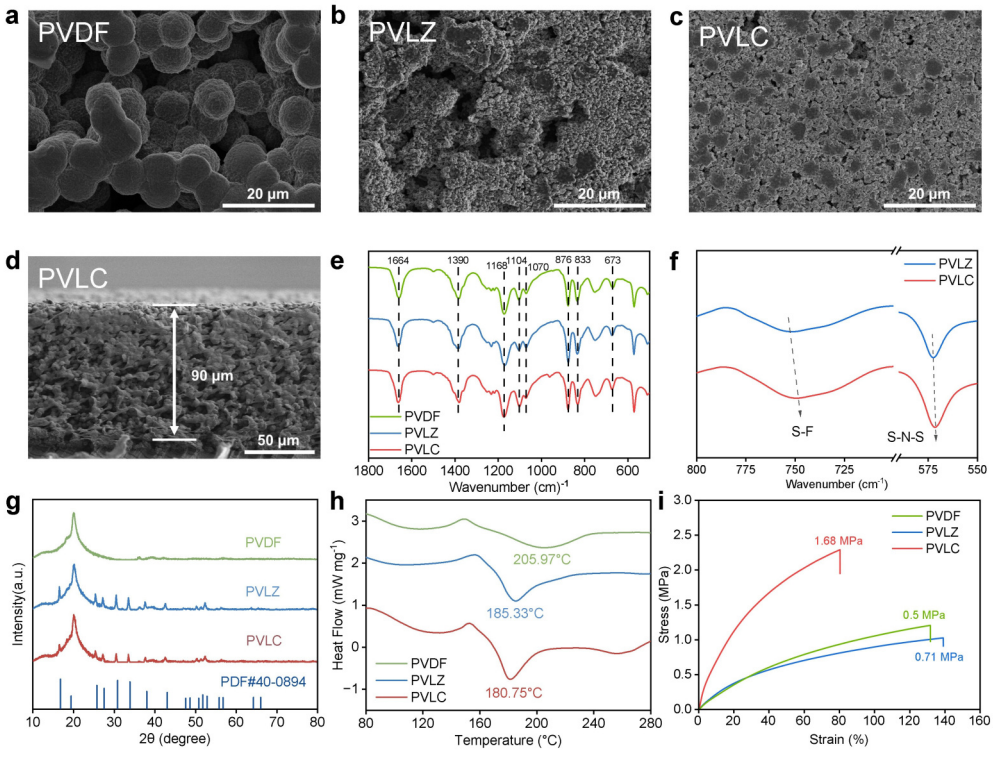

Figure 2 Physicochemical properties of the as-prepared electrolytes. SEM images of the bottom surfaces of the PVDF-only (a), PVDF–LiFSI–LLZTO (PVLZ) (b), and PVDF–LLZTO–crown ether (PVLC) (c) CSEs. (d) Cross-sectional morphology of the PVLC CSE. FTIR (e) and enlarged localized FTIR (f) spectra, XRD patterns (g), differential scanning calorimetry thermograms (h), and tensile strength test curves (i) of the PVDF, PVLZ, and PVLC CSEs.

PVLZ and PVLC electrolytes closely correlated with those of the PVDF-only electrolyte, confirming that the LLZTO filler did not alter the intrinsic polymer structure (Fig. 2e)[26–28]. The stretching vibration peaks of the S–F (751 cm^{-1}) and S–N–S (572 cm^{-1}) groups of the FSI^- anion in the PVLC electrolyte redshifted, indicating weakened interactions between Li^+ and FSI^- (Fig. 2f)[26,29]. Furthermore, X-ray diffraction (XRD) was performed to investigate the structure of the electrolytes. The composite electrolytes containing LLZTO (PVLZ and PVLC) exhibited peaks corresponding to the standard pattern of LLZTO (PDF#40-0894), indicating that LLZTO retained its original crystal structure in the PVDF matrix, thereby ensuring inorganic-phase Li^+ conduction (Fig. 2g).

Thermogravimetric analysis (Figs. S1a and S1b in the ESM) was performed to examine the thermal stability of the CSEs. The results revealed the occurrence of multistage weight loss as the temperature increased. The initial stage (30–180°C) corresponded to the volatilization of residual solvents and adsorbed water, followed by lithium-salt decomposition (between 180 and 300°C) and PVDF-backbone degradation (at >300°C)[30]. The total weight losses observed below 180°C were approximately 12.9% and 14.0% for PVLZ and PVLC, respectively, corresponding to a residual DMF concentration of 11 wt%–12 wt%. The approximately 1.1% additional volatile content in PVLC was attributed to the partial evaporation of free 18-C-6, whereas the majority (~83%) was retained through Li^+ coordination. Differential scanning calorimetry confirmed that the incorporation of 18-C-6 barely influenced the melting point of PVLZ (Fig. 2h), indicating that supramolecular interactions between 18-C-6 and Li^+ mainly influence the ion-coordination environment and interfacial chemistry rather than the bulk thermal degradation pathway. Tensile strength testing revealed significantly enhanced mechanical performance for the 18-C-6-modified electrolyte. The PVLZ CSE exhibited a slightly increased tensile strength (0.71 MPa), whereas the tensile strength of the PVLC CSE significantly increased to 1.68 MPa, following 18-C-6 addition (Fig. 2i).

The Li^+ coordination environment is crucial for regulating electrode/electrolyte interphase composition and ion-transport kinetics, thereby attracting significant interest in solid-state electrolytes. Raman spectroscopy revealed four distinct FSI^- coordination structures in PVDF-based electrolytes: solvent-separated ion pairs (SSIPs; free anion, 721 cm^{-1}), contact ion pairs (CIPs; pairing between one Li^+ and one FSI^-, 730.9 cm^{-1}), ion aggregates (AGG-1; pairing between one Li^+ and two FSI^-, 741 cm^{-1}), and AGG-2 (pairing between one Li^+ and more than two FSI^-, 750 cm^{-1})[31–33]. Quantitative analysis revealed that the 18-C-6-containing PVLC CSE exhibited significantly higher SSIP (14.2%) and CIP (55.9%) proportions compared with PVLZ (12.8% SSIP and 42.4% CIP). Conversely, its relative contents of AGG-1 (10.5% vs. 24.6%) and AGG-2 (19.5% vs. 20.2%) were markedly lower (Figs. 3a–3d). This notable change confirmed that the specific coordination between crown ether cavities and Li^+ effectively weakened Li^+–FSI^- coulombic interactions, suppressing AGG formation. This result correlates with the FTIR spectroscopy results.

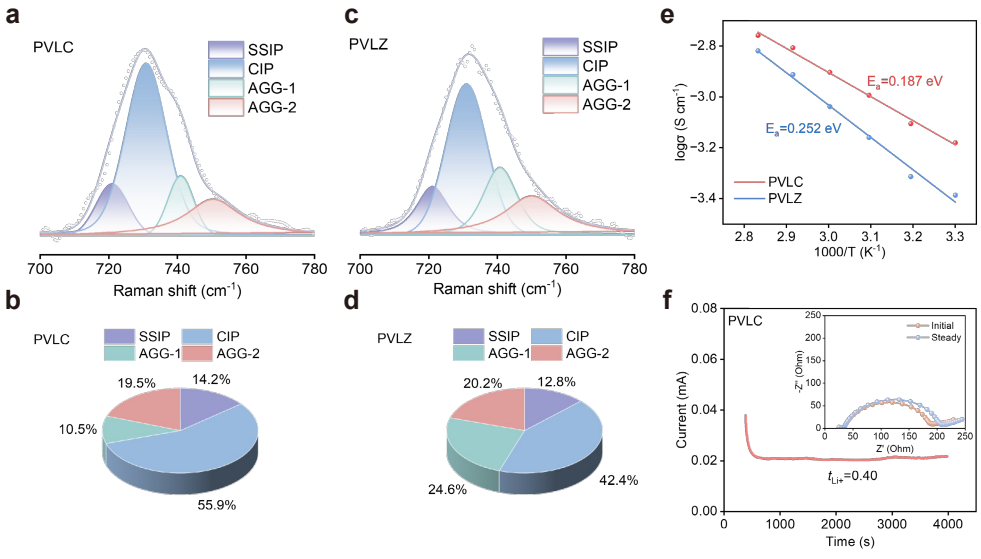

Figure 3 Coordination structures and Li^+-transport performances of PVLZ and PVLC CSEs. Raman spectra of PVLC (a) and PVLZ (c). Relative percentages of different coordination structures calculated from Raman spectra in PVLC (b) and PVLZ (d). (e) Activation energies (E_a) of the PVLC and PVLZ CSEs. (f) Li^+ transference number (t_{Li^+}) of the PVLC CSE.

Electrochemical impedance spectroscopy (EIS) was performed within a temperature range of 30–80°C, revealing a decrease in the activation energy (E_a) from 0.252 eV (PVLZ) to 0.187 eV (PVLC), as shown in Fig. 3e, Figs. S2a and S2b in the ESM. Room temperature EIS analyses confirmed that PVLC exhibited an ionic conductivity of 6.60×10^{-4} S cm^{-1}, representing an approximately 60.6% increase over that of PVLZ (4.11×10^{-4} S cm^{-1}). These results confirmed that PVLC allowed more efficient Li^+ transport (Fig. S2c in the ESM). Integrating the Raman spectroscopy and EIS results revealed that the selective Li^+ coordination by 18-C-6 notably reduced the Li^+–FSI^- interaction strength, lowering the E_a for Li^+ migration and ultimately enhancing ionic conductivity. Moreover, the Li^+ transference number (t_{Li^+}) tests revealed distinct polarization variations for the electrolytes, with the PVLC CSE exhibiting a significantly higher t_{Li^+} (0.40) compared with the PVLZ counterpart (0.11), as shown in Fig. 3f and Fig. S3 in the ESM. This result suggested that 18-C-6 incorporation notably mitigated internal concentration polarization, thereby promoting uniform Li^+ diffusion within the electrolyte.

The electrochemical performances of Li||Li and Li||NCM811 cells were measured to elucidate the effects of the crown ether additive on the PVDF CSEs. Tafel curve analysis demonstrated that the exchange current density of the PVLC CSE increased significantly by 66.8% (0.482 mA cm^{-2}) compared with that of PVLZ (0.289 mA cm^{-2}), underscoring the capability of crown ether to enhance ion-transport kinetics at the interface via the regulated coordination environment and a more stable SEI layer on the Li-anode surface (Fig. 4a). Tests using symmetrical cells (Li||Li) demonstrated a critical current density (CCD) of 2.2 mA cm^{-2} for PVLC electrolyte, which was 2.4 times as high as that of the PVLZ CSE (0.9 mA cm^{-2}), underscoring the effectiveness of the crown ether additive in facilitating uniform Li^+ deposition at the interface (Fig. 4b). Next, the cycling performances of the Li||Li cells were evaluated, further emphasizing the positive influence of the crown ether additive in stabilizing Li anodes. Specifically, the PVLC-containing cell exhibited stable cycling for more than 800 h at consistently low polarization voltages ($\Delta V < 0.05$ V; Fig. 4c). Moreover, the EIS results confirmed that the PVLC CSE exhibited a significantly lower interfacial resistance (100 Ω) compared with PVLZ (200 Ω), confirming the efficient suppression of interfacial side reactions (Fig. S4 in the ESM).

The linear sweep voltammetry results indicated that the electrochemical stability windows of the PVLC and PVLZ CSEs reached 4.64 and 4.25 V, respectively, highlighting the compatibility of the PVLC electrolyte with high-voltage cathodes (Fig. S5 in the ESM). CV analysis of the Li||NCM811 cells (scan rate: 0.05 mV s^{-1}) displayed three pairs of reversible redox peaks within the voltage range of 2.8–4.3 V, corresponding to the multistage phase transitions of NCM811 cathodes: (i) H1→M (3.85/3.69 V), (ii) M→H2 (4.06/3.94 V), and (iii) H2→H3 phase transition (4.30/4.14 V). In addition to the initial irreversible formation of the SEI layer, the CV curves of the PVLC-containing cell displayed high reproducibility and minimal peak-voltage variations (0.02 V) between cycles 2 and 5. These variations were significantly lower than those of its PVLZ counterpart (0.13 V), confirming suppressed electrochemical polarization and enhanced reaction reversibility with PVLC (Fig. 4d and Fig. S6 in the ESM). Rate capability measurements conducted between 2.8 and 4.3 V (from 0.2C to 10C) confirmed that the PVLC electrolyte endowed the Li||NCM811 cell with high discharge capacities of 193.2, 183.3, 171.4, 155.1, 123.7, and 86.1 mAh g^{-1} at rates of 0.2C, 0.5C, 1C, 2C, 5C, and 10C, respectively. Notably, 98.9% capacity retention was achieved when the rate returned to 0.2C (191.1 mAh g^{-1}), demonstrating exceptional rate reversibility and structural stability. Conversely, the PVLZ CSE showed significantly lower capacities under identical experimental conditions (Fig. 4e and Fig. S7 in the ESM).

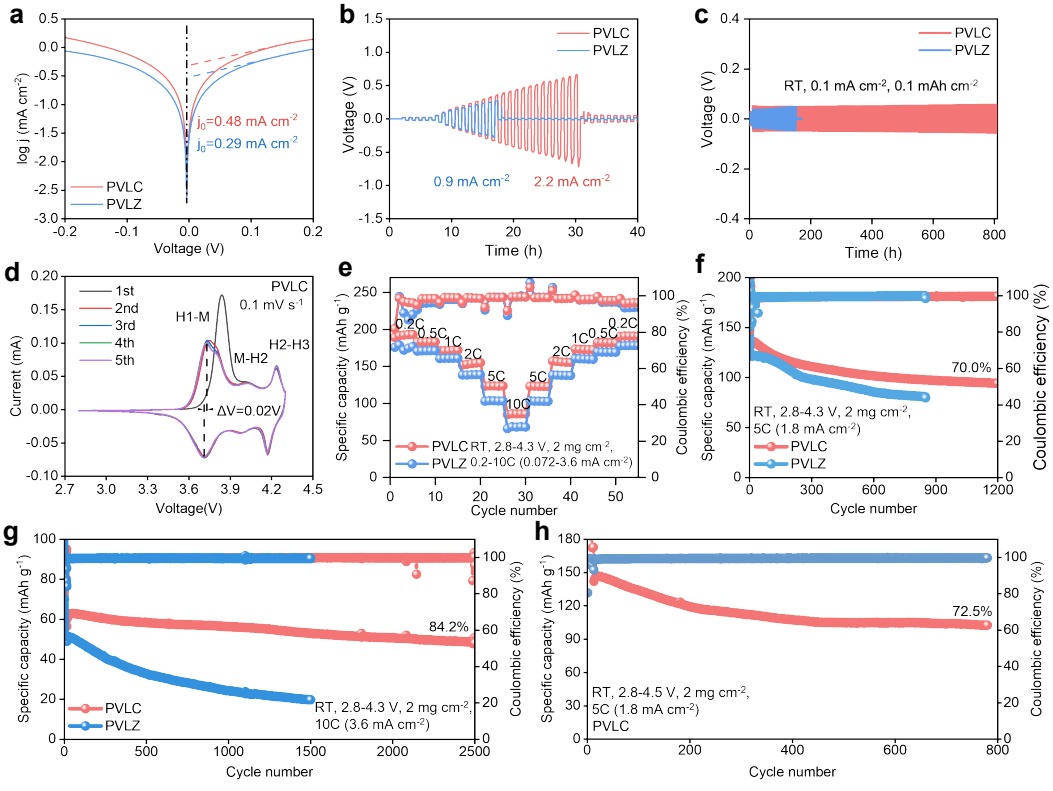

Figure 4 Electrochemical performances of Li||Li and Li||NCM811 cells integrated with PVLZ and PVLC CSEs: Tafel (a) and CCD (b) curves. (c) Long-term cycling performances of the Li||Li cells at 0.1 mA cm^{-2} and 0.1 mAh cm^{-2}. (d) Cyclic voltammetry (CV) curves at different cycle numbers between 2.8 and 4.3 V for the Li||NCM811 cell integrated with a PVLC electrolyte. (e) Rate capabilities of the Li||NCM811 cells between 2.8 and 4.3 V. Cycling stabilities of the Li||NCM811 cells between 2.8 and 4.3 V at 5C (f) and 10C (g) charge/discharge rates. (h) Cycling stabilities of Li||NCM811 cells between 2.8 and 4.5 V at 5C.

The cycling stabilities of the Li||NCM811 cells between 2.8 and 4.3 V and across varying current rates revealed that the PVLC electrolyte delivered an initial capacity of 160.0 mAh g^{-1} at 2C, representing 78.0% capacity retention after 570 cycles, with the coulombic efficiency consistently exceeding 99.3%. Conversely, the PVLZ CSE suffered rapid capacity degradation within 100 cycles owing to electrolyte interfacial instability (Fig. S8 in the ESM), emphasizing the superiority of the PVLC CSE, especially at higher rates. The Li||NCM811 cell integrated with the PVLC CSE retained 70.0% of its initial capacity after 1200 cycles at 5C, whereas the PVLZ electrolyte suffered internal short circuits attributed to dendrite penetration after approximately 800 cycles (Fig. 4f). Remarkably, at 10C, the PVLC-integrated cell demonstrated superior longevity, retaining 84.2% of its initial capacity after 2500 cycles. Conversely, the PVLZ-incorporated cell failed after only 1500 cycles (Fig. 4g). More excitingly, PVLC compares favorably with established state-of-the-art solid-state electrolytes, exhibiting outstanding cycle life and rate performance (Table S1 in the ESM). Moreover, even at a higher charge cut-off voltage (4.5 V), the Li||NCM811 cell containing the PVLC electrolyte still retained 72.5% of its initial capacity after 780 cycles at 5C, maintaining flat voltage plateaus while effectively suppressing polarization (Fig. 4h and Fig. S9 in the ESM).

To further elucidate the root cause of the varied cycle performances of the PVLZ and PVLC CSEs, the interfacial chemistry of the cycled Li anodes was investigated after 50 cycles in Li||Li symmetrical cells. First, XPS was performed to analyze the chemical composition and spatial distributions of the SEI formed on the Li-anode surface. High-resolution C 1s XPS spectra (Figs. 5a and 5d) revealed characteristic peaks corresponding to C–C (284.8 eV), C–O (286.1 eV), C=O (288.0 eV), and Li_2CO_3 (290.1 eV)[30,34]. The emergence of C–O/C=O groups was attributed to the decomposition of residual DMF solvents. Notably, the C–O/C=O peaks exhibited significantly lower intensities for the PVLC electrolyte than for PVLZ. The intensity further reduced after etching for 60 s, demonstrating the effectiveness of crown ether additives in suppressing solvent decomposition. The F 1s XPS spectra (Figs. 5b and 5e) displayed two characteristic peaks corresponding to FSI^- decomposition products (687.9 eV) and LiF (685.1 eV)[22]. Depth profiling confirmed that PVLC generated strong LiF signals within the SEI inner layer by regulating ion transport therein, ultimately achieving uniform Li^+ flux. Additionally, the N 1s XPS spectra demonstrated that PVLC contained a higher amount of Li_3N (399.1 eV) compared with the PVLZ (Figs. 5c and 5f)[35, 36]. As established, Li_3N exhibits high ionic conductivity, contributing to the formation of a robust SEI layer with enhanced mechanical strength and ionic-transport capability when paired with LiF. Thus, the crown ether additive facilitates preferential FSI^- decomposition to form an inorganic LiF/Li_3N layer and inhibits DMF decomposition to decrease the amount of organic components, thereby effectively mitigating Li dendritic growth and

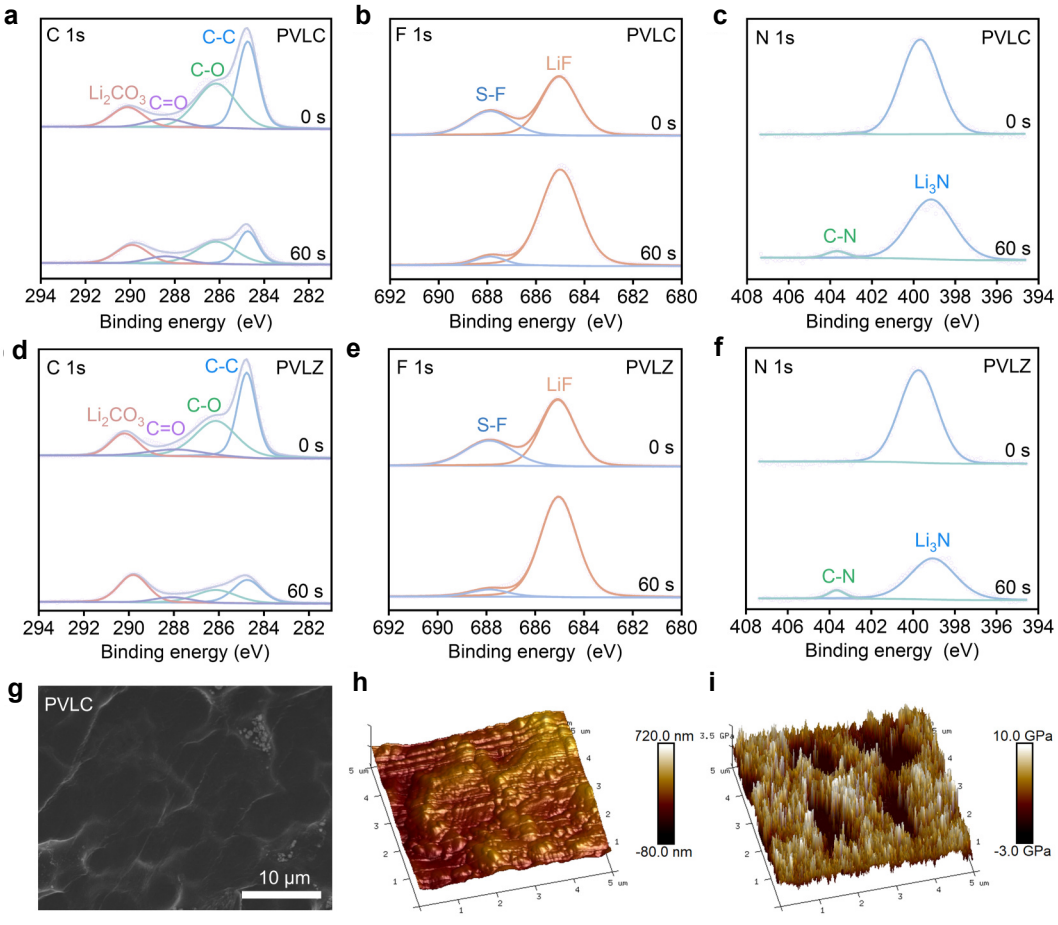

Figure 5 Interfacial chemistry of cycled Li anodes. High-resolution C 1s (a, d), F 1s (b, e), and N 1s (c, f) X-ray photoelectron spectroscopy (XPS) spectra of the cycled Li anode integrated with PVLC (a–c) and PVLZ (d–f) CSEs. (g) SEM image of the cycled Li anode. Three-dimensional surface morphology (h) and Young's modulus (i) of the SEI on Li anodes after 50 cycles with the PVLC electrolyte.

continuous interfacial side reactions, which are crucial for high-rate, long-cycle stability.

Furthermore, the SEM images of the Li anodes after 50 cycles were investigated to reveal the differences between the surface morphologies of PVLC and PVLZ CSEs (Fig. 5g and Fig. S10 in the ESM). Evidently, the PVLZ electrolyte induced extensive uneven Li deposition and noticeable surface roughness due to lithium dendrite growth and the accumulation of dead lithium. Conversely, the PVLC electrolyte exhibited uniform, compact surface morphologies, indicating its capability to regulate the lithium-deposition behavior. Furthermore, atomic force microscopy revealed that the surface roughness of the Li anodes obtained from the PVLC electrolyte reduced to 30.1 nm, which was approximately 68% lower than that of the PVLZ CSE exhibiting a high value of 95.4 nm (Fig. 5h and Fig. S11a in the ESM). As shown in Fig. 5i and Fig. S11b in the ESM, the Young's modulus of the PVLC SEI reached 4.14 GPa, which was significantly higher than that of PVLZ (1.65 GPa). These results demonstrate that the 18-C-6 (crown ether) additive effectively improves the mechanical strength of the SEI, greatly enhancing the reversibility of lithium plating and stripping and ultimately prolonging the cycle lifespan of LMBs.

4 Conclusion

In summary, a supramolecular ligand is proposed for the improvement of the ionic conductivity of PVDF-based CSEs and the regulation of their interfacial stability. The introduction of an 18-C-6 additive facilitates LiFSI dissociation and increases the free Li^+ concentration by leveraging its electron-rich cyclic cavity that selectively coordinates with Li^+, enabling rapid Li^+ transport in the PVLC electrolyte. Moreover, the interaction between 18-C-6 and Li^+ induces a uniform Li^+ flux, which simultaneously suppresses solvent (DMF) decomposition and Li dendrite growth. Consequently, the experimental Li||Li cells achieve a prolonged cycle lifespan of over 800 h at 0.1 mA cm^{-2}. Furthermore, the PVLC CSE exhibits a broad electrochemical stability window extending to 4.64 V. This high stability endows NCM811||Li cells with excellent cycling stability, surpassing 570, 1200, and 2500 cycles at 2C, 5C, and 10C, respectively. Moreover, the cycle lifespan of the NCM811||Li cells is nearly 800 cycles at 5C even at a high charge cut-off voltage of 4.5 V. This study provides valuable insights for developing PVDF solid-state electrolytes with rapid Li^+-transport kinetics and excellent interfacial stability toward high-performance solid-state LMBs.

Acknowledgements

None.

Author contribution statement

Yan-Bing He and Hai Su conceived and supervised the project. Qian-Nan Zhu, Kang-Rui Ren, Jun-Yao You, Hai Su, and Yan-Bing He designed the experiments. Qian-Nan Zhu, Jun-Yao You and Kang-Rui Ren performed the experiments. Qian-Nan Zhu, Kang-Rui Ren, Zhen-Han Xie, Hai Su and Yan-Bing He wrote the initial manuscript which was reviewed and edited by all the authors. All the authors have approved the final manuscript.

Data availability

The data that support the findings of this study are available from the corresponding author upon reasonable request.

Declaration of competing interest

The corresponding author Yan-Bing He is the Executive Editor-in-Chief of this journal, but he is not involved in the peer review or decision of this article. The other contributing authors report no conflicts of interest in this work.

Funding

This work was supported by the National Key Research and Development Program of China (Grant No. 2021YFF0500600), the National Science Fund for Distinguished Young Scholars (Grant No. 52325206), the National Natural Science Foundation of China (Grant Nos. U2001220, 52203298, and 523B2022), the Shenzhen Technical Plan Project (Grant Nos. RCJC20200714114436091, JCYJ20220530143012027, JCYJ20220818101003008, and JCYJ20220818101003007), Energy Revolution S&T Program of Yulin Innovation Institute of Clean Energy (Grant No. E511060817), and the Tsinghua Shenzhen International Graduate School-Shenzhen Pengrui Young Faculty Program of Shenzhen Pengrui Foundation (Grant No. SZPR2023006).

Use of AI statement

None.

References

[1] Lu, G. X., Nai, J. W., Luan, D. Y., Tao, X. Y., Lou, X. W. (2023). Surface engineering toward stable lithium metal anodes. *Sci. Adv.* 9, eadf1550.

[2] Luo, D., Li, M., Zheng, Y., Ma, Q. Y., Gao, R., Zhang, Z., Dou, H. Z., Wen, G. B., Shui, L. L., Yu, A. P., et al. (2021). Electrolyte design for lithium metal anode-based batteries toward extreme temperature application. *Adv. Sci.* 8, 2101051.

[3] Feng, Y., Zhou, L. M., Ma, H., Wu, Z. H., Zhao, Q., Li, H. X., Zhang, K., Chen, J. (2022). Challenges and advances in wide-temperature rechargeable lithium batteries. *Energy Environ. Sci.* 15, 1711–1759.

[4] Lu, X., Wang, Y. M., Xu, X. Y., Yan, B. G., Wu, T., Lu, L. (2023). Polymer-based solid-state electrolytes for high-energy-density lithium-ion batteries-review. *Adv. Energy Mater.* 13, 2301746.

[5] Fan, L. Z., He, H. C., Nan, C. W. (2021). Tailoring inorganic-polymer composites for the mass production of solid-state batteries. *Nat. Rev. Mater.* 6, 1003–1019.

[6] Liu, D. H., Bai, Z. Y., Li, M., Yu, A. P., Luo, D., Liu, W. W., Yang, L., Lu, J., Amine, K., Chen, Z. W. (2020). Developing high safety Li-metal anodes for future high-energy Li-metal batteries: strategies and perspectives. *Chem. Soc. Rev.* 49, 5407–5445.

[7] Wang, Q., Wang, H. C., Wu, J. Y., Zhou, M. Y., Liu, W., Zhou, H. H. (2021). Advanced electrolyte design for stable lithium metal anode: from liquid to solid. *Nano Energy* 80, 105516.

[8] Zhao, Q., Stalin, S., Zhao, C. Z., Archer, L. A. (2020). Designing solid-state electrolytes for safe, energy-dense batteries. *Nat. Rev. Mater.* 5, 229–252.

[9] Aziam, H., Larhrib, B., Hakim, C., Sabi, N., Ben Youcef, H., Saadoune, I. (2022). Solid-state electrolytes for beyond lithium-ion batteries: a review. *Renew. Sustain. Energy Rev.* 167, 112694.

[10] Reinoso, D. M., Frechero, M. A. (2022). Strategies for rational design of polymer-based solid electrolytes for advanced lithium energy storage applications. *Energy Storage Mater.* 52, 430–464.

[11] Liu, S. J., Zhou, L., Zhong, T. J., Wu, X., Neyts, K. (2024). Sulfide/polymer composite solid-state electrolytes for all-solid-state lithium batteries. *Adv. Energy Mater.* 14, 2403602.

[12] Liu, J. F., Wu, Z. Y., Stadler, F. J., Huang, Y. F. (2023). High dielectric poly(vinylidene fluoride)-based polymer enables uniform lithium-ion transport in solid-state ionogel electrolytes. *Angew. Chem. Int. Ed.* 62, e202300243.

[13] Huang, Y. F., Gu, T., Rui, G. C., Shi, P. R., Fu, W. B., Chen, L., Liu, X. T., Zeng, J. P., Kang, B. H., Yan, Z. C., et al. (2021). A relaxor ferroelectric polymer with an ultrahigh dielectric constant largely promotes the dissociation of lithium salts to achieve high ionic conductivity. *Energy Environ. Sci.* 14, 6021–6029.

[14] Zhang, X., Han, J., Niu, X. F., Xin, C. Z., Xue, C. J., Wang, S., Shen, Y., Zhang, L., Li, L. L., Nan, C. W. (2020). High cycling stability for solid-state Li metal batteries via regulating solvation effect in poly(vinylidene fluoride)-based electrolytes. *Batteries Supercaps* 3, 876–883.

[15] Zhu, J. X., He, S., Tian, H. Y., Hu, Y. M., Xin, C., Xie, X. X., Zhang, L. P., Gao, J., Hao, S. M., Zhou, W. D. et al. (2023). The influences of DMF content in composite polymer electrolytes on Li^+-conductivity and interfacial stability with Li-metal. *Adv. Funct. Mater.* 33, 2301165.

[16] Liang, Y., Guan, S. D., Xin, C. Z., Wen, K. H., Xue, C. J., Chen, H. T., Liu, S. J., Wu, X. B., Yuan, H. C., Li, L. L. et al. (2022). Effects of molecular weight on the electrochemical properties of poly(vinylidene difluoride)-based polymer electrolytes. *ACS Appl. Mater. Interfaces* 14, 32075–32083.

[17] Yu, J., Liu, J. P., Lin, X. D., Law, H. M., Zhou, G. D., Kwok, S. C. T., Robson, M. J., Wu, J. X., Ciucci, F. (2021). A solid-like dual-salt polymer electrolyte for Li-metal batteries capable of stable operation over an extended temperature range. *Energy Storage Mater.* 37, 609–618.

[18] Arrese-Igor, M., Martinez-Ibañez, M., del Amo, J. M. L., Sanchez-Diez, E., Shanmukaraj, D., Dumont, E., Armand, M., Aguesse, F., López-Aranguren, P. (2022). Enabling double layer polymer electrolyte batteries: overcoming the Li-salt interdiffusion. *Energy Storage Mater.* 45, 578–585.

[19] Zhou, H. Y., Ou, Y., Yan, S. S., Xie, J., Zhou, P., Wan, L., Xu, Z. A., Liu, F. X., Zhang, W. L., Xia, Y. C. et al. (2023). Supramolecular polymer ion conductor with weakened li ion solvation enables room temperature all-solid-state lithium metal batteries. *Angew. Chem. Int. Ed.* 62, e202306948.

[20] Wang, D., Xie, H., Liu, Q., Mu, K. X., Song, Z. N., Xu, W. J., Tian, L., Zhu, C. Z., Xu, J. (2023). Low-cost, high-strength cellulose-based quasi-solid polymer electrolyte for solid-state lithium-metal batteries. *Angew. Chem. Int. Ed.* 62, e202302767.

[21] Yang, K., Chen, L. K., Ma, J. B., Lai, C., Huang, Y. F., Mi, J. S.,

Biao, J., Zhang, D. F., Shi, P. R., Xia, H. Y. (2021). Stable interface chemistry and multiple ion transport of composite electrolyte contribute to ultra-long cycling solid-state $LiNi_{0.8}Co_{0.1}Mn_{0.1}O_2$/lithium metal batteries. *Angew. Chem. Int. Ed.* 60, 24668–24675.

[22] Wu, Z. Y., Li, S. F., Huang, Y. F. (2024). Stabilizing poly (vinylidene fluoride) solid-state electrolytes/lithium metal interface by constructing an ultrathin interface layer to inhibit the electron transfer. *Energy Storage Mater.* 68, 103330.

[23] Wang, L. N., Menakath, A., Han, F. D., Wang, Y., Zavalij, P. Y., Gaskell, K. J., Borodin, O., Iuga, D., Brown, S. P., Wang, C. S. et al. (2019). Identifying the components of the solid-electrolyte interphase in Li-ion batteries. *Nat. Chem.* 11, 789–796.

[24] Zhou, Y. F., Su, M., Yu, X. F., Zhang, Y. Y., Wang, J. G., Ren, X. D., Cao, R. G., Xu, W., Baer, D. R., Du, Y. G. et al (2020). Real-time mass spectrometric characterization of the solid-electrolyte interphase of a lithium-ion battery. *Nat. Nanotechnol.* 15, 224–230.

[25] Wu, A. H., Zhang, S. J., Li, Q. H., Xue, W. X., Li, C. Y., Xi, B. J., Mao, W. T., Bao, K. Y., Xiong, S. L. (2025). Multifunctional crown ether additive regulates desolvation process to achieve highly reversible zinc-metal batteries. *Adv. Energy Mater.* 15, 2404450.

[26] Dai, C., Weng, M. W., Cai, B. W., Liu, J. F., Guo, S. K., Xu, H., Yao, L., Stadler, F. J., Li, Z. M., Huang, Y. F. (2024). Ion-conductive crystals of poly(vinylidene fluoride) enable the fabrication of fast-charging solid-state lithium metal batteries. *Energy Environ. Sci.* 17, 8243–8253.

[27] Gao, M. J., Zhou, D., Wen, B., Zhu, S., Ni, J. F. (2025). Weak interaction in polymer electrolyte enables fast charging of solid-state lithium batteries. *Adv. Funct. Mater.* 35, 2500727.

[28] Li, Y. S., Yuan, W. H., Hu, Z., Shen, Y. B., Wu, G. S., Cong, F., Fu, X. Z., Lu, F., Li, Y. L., Liu, P. X. et al. (2025). Constructing PVDF-based polymer electrolyte for lithium metal batteries by polymer-induced phase structure adjustment strategy. *Adv. Funct. Mater.* 35, 2424763.

[29] Liu, Q. Y., Yang, G. J., Li, X. Y., Zhang, S. M., Chen, R. J., Wang, X. F., Gao, Y. R., Wang, Z. X., Chen, L. Q. (2022). Polymer electrolytes based on interactions between [solvent-Li+] complex and solvent-modified polymer. *Energy Storage Mater.* 51, 443–452.

[30] Yang, W. J., Liu, Y. W., Sun, X. Y., He, Z. Y., He, P., Zhou, H. S. (2024). Solvation-tailored PVDF-based solid-state electrolyte for high-voltage lithium metal batteries. *Angew. Chem. Int. Ed.* 63, e202401428.

[31] Ma, Y. T., Chen, L. K., Li, Y. H., Li, B. Y., An, X. F., Cheng, X., Su, H., Yang, K., Xiao, G. Y., Zhao, Y. et al. (2025). Mesoscale polymer regulation for fast-charging solid-state lithium metal batteries. *Energy Environ. Sci.* 18, 3730–3739.

[32] Chen, L. K., Gu, T., Mi, J. S., Li, Y. H., Yang, K., Ma, J. B., An, X. F., Jiang, Y. Y., Zhang, D. F., Cheng, X. et al. (2025). Homogeneous polymer-ionic solvate electrolyte with weak dipole-dipole interaction enabling long cycling pouch lithium metal battery. *Nat. Commun.* 16, 3517.

[33] Yang, K., Ma, J. B., Li, Y. H., Jiao, J. Y., Jiao, S. Z., An, X. F., Zhong, G. M., Chen, L. K., Jiang, Y. Y., Liu, Y. et al. (2024). Weak-interaction environment in a composite electrolyte enabling ultra-long-cycling high-voltage solid-state lithium batteries. *J. Am. Chem. Soc.* 146, 11371–11381.

[34] An, X. F., Liu, Y., Yang, K., Mi, J. S., Ma, J. B., Zhang, D. F., Chen, L. K., Liu, X. T., Guo, S. K., Li, Y. H. et al. (2024). Dielectric filler-induced hybrid interphase enabling robust solid-state li metal batteries at high areal capacity. *Adv. Mater.* 36, 2311195.

[35] Zhang, S. X., Liu, H., Liu, Z. B., Zhao, Y. J., Yan, J., Zhang, Y. Q., Liu, F. Y., Liu, Q., Liu, C., Sun, G. et al. (2024). Non-resonant structure induces n-rich solid electrolyte interface toward ultra-stable solid-state lithium-metal batteries. *Adv. Funct. Mater.* 34, 2401377.

[36] Liu, M. Q., Cai, J. M., Zuo, Y. Z., Luo, W. H., Huang, Y. F., Qiu, R. X., Luo, Y. Y., Lei, J., Yan, H., Yan, W. et al. (2025). Constructing continuously-distributed and crystalline-NaF-rich SEI on hard carbon anode through binder chemistry for high-performance sodium-ion batteries. *Adv. Mater.* 37, e05368.